Characterisation of fluid-structure interaction for water impact of composite panels

Mark A. Battley* and Tom D. Allen
Centre for Advanced Composite Materials, Department of Mechanical Engineering, Unversity of Auckland, Private Bag 92019, Auckland, New Zealand

ABSTRACT

Hydrodynamic loads can be very significant for high performance marine vessels. Water impact of panels, known as "slamming", typically generates high magnitude short duration pressure pulses that move across the structure. In the case of compliant panels there can be significant coupling between the pressures and the structural responses. While there has been significant development of numerical methods to simulate this type of fluid-structure interaction there is only very limited experimental data available for validation of the simulation approaches. This paper describes an experimental study of sandwich composite panels subjected to water slamming impacts. The results demonstrate that compliant panels subjected to water slamming impacts experience different pressures than rigid panels, and have different structural responses than predicted by traditional uniform pressure based analysis approaches. The study also characterizes the significant effects that the dimensions of pressure transducers and data acquisition sampling rates have on the measured pressures.

Keywords: Water Slamming, Experimental Measurement, Sandwich Composite, Fluid-Structure Interaction, Validation.

1. INTRODUCTION

Composite materials are widely used for high performance marine vessels, including in naval applications. Hydrodynamic loads can be very significant for these structures, particularly for high-speed craft. The usual design approach for hull panels treats them as being subjected to a uniformly distributed static pressure whose magnitude is given by empirical formulae. This approach is embedded within many scantling codes and is also used for analytical and numerical analyses of panels. In reality the water pressure acting on most hull structures is neither uniformly distributed nor static. In particular, slamming events (Figure 1) typically generate high magnitude pressure pulses of very short duration that move across the panel as the hull enters the water. In the case of compliant panels there can be significant coupling between the applied pressures and the panel structural responses. While there has been significant development of numerical methods to simulate this type of fluid-structure interaction there is only very limited experimental data available for validation and refinement of the simulation approaches.

*Corresponding author, Mark A. Battley, Email: m.battley@auckland.ac.nz

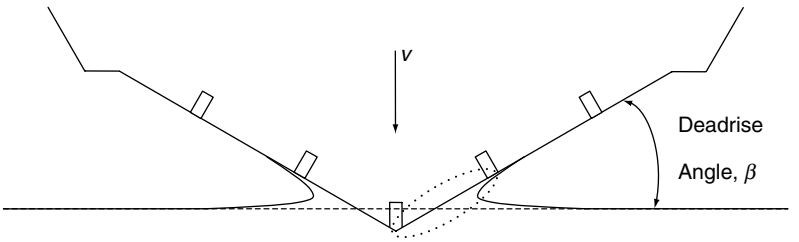

Figure 1 Cross-section of marine vessel undergoing hull slamming.

This research investigates the loading and responses of compliant composite panels subjected to water slamming impacts. Testing has been carried out on flexible composite panels with varying flexural and shear rigidity as well as a nominally rigid panel. The tests were conducted under constant impact velocity using a Servo-hydraulic Slam Testing System. Instrumentation included piezoelectric pressure transducers, resistance strain gauges, a load cell, accelerometers and displacement transducers to measure panel deflection. The results have been analysed to characterize the structural responses of the panels to the slamming loads and identify the significance of hydroelastic phenomena experienced by the flexible panels. The panel responses during a slamming event are compared to those predicted by traditional analysis approaches based on uniform pressure loads. The study also characterizes the significant effects that the dimensions of pressure transducers and data acquisition sampling rates have on the measured pressures. This is of crucial importance if the data is to be utilised for validation of simulation approaches.

2. METHODOLOGY

2.1. TEST SYSTEM

The testing system used in this study (see Figure 2) is known as the Servo-hydraulic Slam Testing System (SSTS). This was custom designed and developed by Industrial Research Limited, Auckland, NZ and the University of Auckland and utilises a sophisticated high-speed servo-hydraulic system to control the motion of a panel structure during impact with the water. Details of the system are described in a 2011 paper by Battley and Allen [1].

The SSTS uses a cylindrical water tank with a diameter of 3.5 m and a water depth of typically 1.4 m, giving a fluid domain of 13,500L. A steel frame supports the hydraulic ram, manifold, servo-valve, accumulators and associated plumbing above the tank. The specimen fixture (see Figure 3), which is attached to the hydraulic ram, slides on vertical rails and hence moves in one degree of freedom as shown in Figure 4. The system is designed for testing panel specimens approximately 1000 × 500 mm. Two hydraulic accumulators supply oil to the ram and the velocity is controlled by a servo-valve and a closed-loop PID controller using position and acceleration feedback. Three vertical panels, two on the sides and one behind the panel constrain the flow along the panel (see Figure 4). The servo-hydraulic ram has a stroke of 1.4 m, typically including approximately 0.4 m travelled in air prior to impact, then up to 0.5 m travelled during the impact event, and a further 0.5 m if required for the specimen to stop. The SSTS can achieve velocities of up to approximately 10 m/s. The specialised servo-hydraulic hardware is controlled by a MOOG™ MSC 3000 electronic controller and custom developed software to achieve the required combination of high velocity, force, and accurate control of motion during the slamming event.

Figure 2 Servohydraulic Slam Testing System.

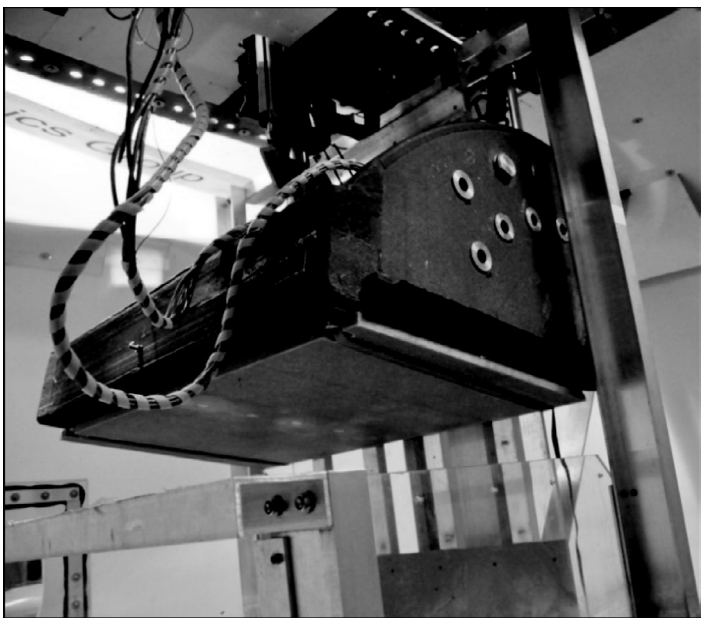

Figure 3 Specimen and fixture.

The closed loop control system uses feedback from the ram displacement transducer and from an accelerometer at the end of the ram to achieve the targeted motion. The control parameters can be defined in different ways depending on the complexity of the desired

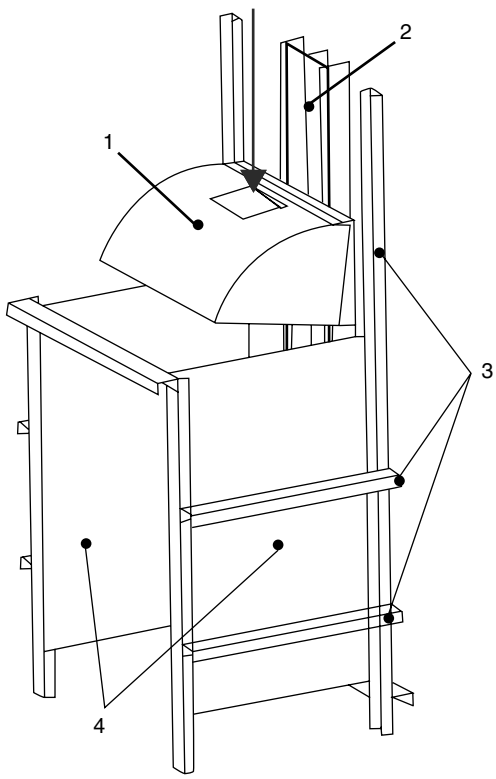

Figure 4 Schematic of specimen fixture and flow control panels 1-Specimen Fixture, 2-Linear bearings and tracks, 3-Aluminium support frame, 4-Flow restriction panels.

motion. In the simplest case, for a constant velocity the primary inputs are initial acceleration from rest, target velocity for the constant speed stage, then a de-acceleration rate at the end of the test. There are additional input parameters to define the duration of each phase and filtering settings for the feedback signals. For more complex velocity profiles the command signal can be defined by a table of time-displacement inputs. This enables an arbitrary motion to be defined, such as increasing or decreasing velocity during the test, or the input of a velocity profile measured from an actual vessel in sea-trials.

At higher velocities and low deadrise angles the slamming impact can occur in a shorter time than the servovalve and control system are able to adequately respond. To improve the performance of the system for these situations the control system enables a feed-forward command to be defined, input as a table of time versus additional valve opening commands. This has the effect of starting to open the servovalve just before the slamming impact occurs, so that the required valve opening and hence applied force can be achieved within the duration of the slamming event. The correct settings for the feed-forward command are determined by iterative testing.

The SSTS has been used for many studies on slamming behavior. Battley and Stenius [2] conducted a series of experiments on a single curvature sandwich core panel. A transient Finite Element Analysis (FEA) simulation was compared with the experiments. The FEA simulation used a simplified pressure distribution. The maximum pressure was calculated from Stavovy and Chuang's semi-empirical peak pressure formula [3], and the residual pressure was based on Payne's mean pressure calculations [4]. The rise and fall times were the only variables obtained from experimental data. The results showed good correlation between experimental and FEA solutions for all values except strain, which the authors attribute to rigid body inertial motions the FEA solution does not account for. Breder [5] conducted a methodical set of experiments characterising the pressures exerted on a rigid half wedge impacting at constant velocity using the SSTS.

Downs-Honey, Edinger and Battley [6] used the SSTS to investigate how well these mechanical property tests, such as ASTM C273 and ASTM C393, predicted the properties that are exhibited during slamming. Their work focused on comparing mechanical properties obtained through 4-point bending and plate shear tests, or from manufacturers' datasheets, with the panel responses during slamming. Their results showed that some cores, such as the Nomex and SuperLite™ Balsa performed as expected based on the dynamic material properties obtained. However both the PVC foam cores significantly exceeded their predictions, the authors believe this was due to increased energy absorption at higher strain rates.

Following on from Downs-Honey et al. [6], Battley and Lake [8] looked experimentally at how the response of a sandwich panel subjected to slamming loads varies from the same panel subjected to a uniform static load. Design specifications and scantling codes often make this simplification; as a result of Battley and Lake's work [7] the inefficacies in making this simplification were demonstrated. Their conclusion was that slamming induced much higher shear loading and deflections than static panel theory would predict. The study described in this study extends this research.

2.2. INSTRUMENTATION

During the impacts the applied load and corresponding panel responses are measured and recorded using a variety of load cells, strain gauges, displacement transducers and pressure transducers. A modular National Instruments™ compact data acquisition system (NI cDAQ 9178) and National Instruments LabVIEW software is used to record data from a set of transducers during each test. Typically data is sampled at rates of 10 to 30 kHz, dependant on the impact speed. Specifications of the transducers used are given in Table 1. The position of the transducers is shown in Figure 5.

2.3. SPECIMENS

For this test series the specimens had external dimensions of 565 mm by 1030 mm, with an unsupported region between simply supported edges of 500 × 1000 mm. The laminates (see Table 2) consisted of three panels with glass fibre/epoxy skins and different types of polymeric foam cores (G-R63.80, G-R63.140 and G-C70.130) and a carbon fibre/epoxy skin panel with a PVC foam core (C-C70.140). The specimens were designed to have different flexural and shear stiffnesses, resulting in the shear factors (Equation (1)) shown in Table 2.

$$\theta = D / L^2 S \tag{1}$$

Where; D = flexural rigidity, L = width of panel and S = shear stiffness.

Table 1 Transducer specifications.

Parameter	Manufacturer	Model	Signal conditioning
Total applied load	Precision transducers	LPC10t	NI 9237 cDAQ Module
Ram displacement	Vishay	139 L	PCB-483B03 24v DC Supply
Ram acceleration	PCB piezotronics	Series 308B	PCB-483B03 24v DC Supply
Panel strains	Measurements group	Various, typically 6 mm gauge length	NI 9237 cDAQ Module
Panel displacements	Schaevitz	LCIT-1000 LCIT-2000	DC Supply ± 12v
Fluid pressure	PCB piezotronics	W113A26/003C20	NI 9234 cDAQ Module

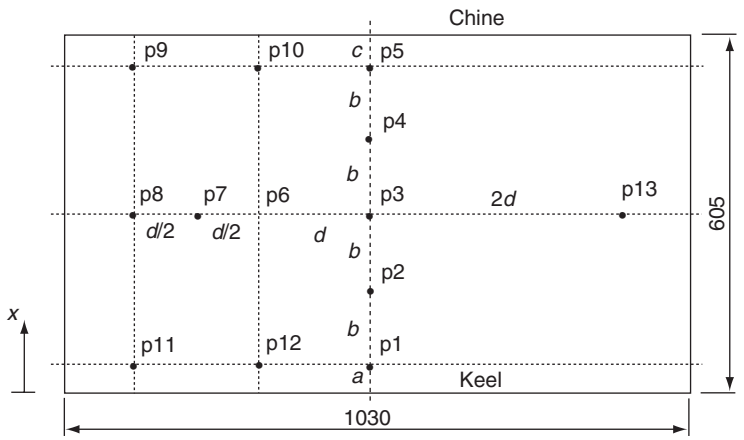

Figure 5 Schematic of the panel showing positions of pressure measurement points, a = 55, b = 107.5, c = 125 and d = 200 mm.

TABLE 2 Specimen details.

Materials	Glass/Cross-linked PVC Core G-C70.130	Carbon/Cross-linked PVC Core C-C70.130	Glass/Linear PVC Core G-R63.80	Glass/Linear PVC Core G-R63.140
Reinforcement	Glass Fibre	Carbon Fibre	Glass Fibre	Glass Fibre
Orientation	$(0/\pm 45/90)_4$	$(0/90)_5$	$(0/\pm 45/90)_4$	$(0/\pm 45/90)_4$
Core Material	PVC, Airex C70.130	PVC, Airex C70.130	PVC, Airex R63.80	PVC, Airex R63.140
Dimensions				
Skin Thickness	2.5 mm	2.5 mm	2.5 mm	2.5 mm
Core Thickness	15 mm	15 mm	20 mm	20 mm
Properties				
Flexural Rigidity	6,740 Nm	25,500 Nm	11,264 Nm	11,264 Nm
Shear Stiffness	960,000 N/m	960, 000 N/m	1,063,125 N/m	1,873,125 N/m
Shear factor	0.028	0.106	0.024	0.042

3. APPLIED PRESSURES

3.1. COMPARISON OF RIGID & FLEXIBLE PANELS

Figure 6 compares the transient pressures at transducers P1, P3 and P5 (positions as in Figure 5) in a 3 m/s flexible panel test (G-C70.130) to those of a rigid panel structure. The pressure magnitudes and profile at P1 are very similar for the rigid and deformable panels. This is expected as the deformable panel does not deflect significantly until later in the slamming event. The pressures at P3 (panel centre) are significantly different, particularly the residual pressure which is initially higher for the deformable panel, then reduces to a similar level as the rigid panel at the end of the slamming event. At P5 the peak pressure for the deformable panel is higher than that for the rigid panel while the residual is similar.

These differences are believed to be related to the transient kinematic behaviour of the deformable panel during the slamming event. In this case the centre of the deformable panel deforms up to a maximum of approximately 8 mm, reducing the velocity of the panel relative to the water to approximately 2.2 m/s, thereby reducing the peak pressure. As the panel reaches its maximum deflection its relative velocity increases back to the velocity of the testing fixture, then increases further as the panel rebounds towards, and then beyond its initial position. This is believed to be the cause of the increased residual pressure at the panel centre.

The deformation in the vicinity of P5 (close to the panel boundary) is also significant, reaching approximately 4.3 mm. This is measured approximately 35 mm from the chine boundary support, demonstrating that there is appreciable rotation of the panel in this region, presumably due to transverse shear deformation of the panel. The deformation has the effect of reducing the local deadrise angle, thereby increasing the local pressure.

3.2. EFFECT OF SENSOR SIZE & SAMPLING RATE

Measurement of applied pressures allows for direct comparison of load cases between not only experimental impacts, but also with numerical simulations and theoretical predictions. A key factor when comparing experimentally obtained data with alternative prediction methods is ensuring that the pressures are correlated for the physical dimensions of the transducer's sampling area and the sampling rate of the data acquisition system. A theoretical solution for the pressure distribution on a plate was developed by Wagner [8]. The equation for the pressure distribution along the width of the plate, for a constant velocity impact is

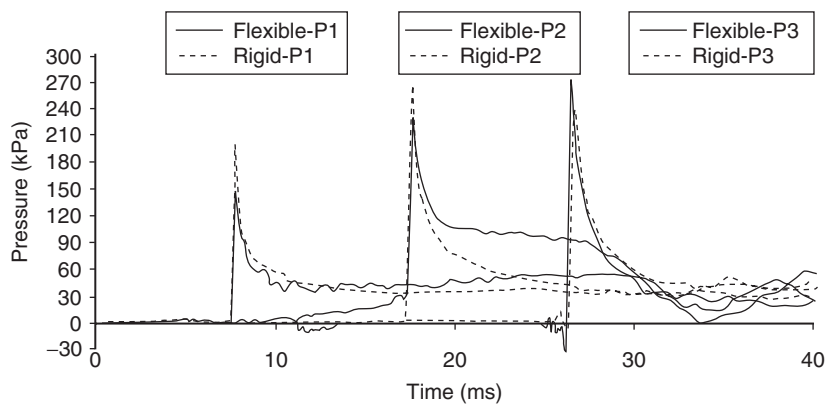

Figure 6 Pressure comparison between rigid and deformable sandwich panel (G-C70.130) for water slamming impact at 3 m/s and a deadrise angle of 10 deg.

given in equation (2), where v_y is the vertical velocity of the plate, β is the deadrise angle of the plate, ρ is the density of water, t is the time since the start of the impact and x is the spanwise location of interest.

$$P_W = \frac{\pi^2 v_y{}^2 \rho t}{(2\tan\beta)^2 \sqrt{\left(\frac{\pi v_y t}{2\tan\beta}\right)^2 - x^2}} \tag{2}$$

The peak value for the pressure is given by equation (3). Wagner's prediction does not prescribe the distribution prior to this peak. For the purposes of this research a linear rise has been used, from $P_W(c) = 0$ to $P_W(x_{P_{\max}}) = P_{\max}$. This leads to equation (5) for the pressure distribution prior to the peak value.

$$P_{\max} = \frac{1}{2}\rho\left(\frac{\pi v_y}{2\tan\beta}\right)^2 \tag{3}$$

$$x_{p\max} = \sqrt{c(t) - \left(\frac{4c(t)\tan\beta}{\pi}\right)^2} \tag{4}$$

$$P_L = \frac{P_{\max}}{\frac{x}{\sqrt{1 - \frac{16(\tan\beta)^2}{\pi^2}}} - x} - (c(t) - x) \tag{5}$$

These two pressure distributions, P_{linear} and P_W need to be integrated over the area of the pressure transducer in order be directly comparable with the experimental data. Equations (6) and (7) give the equations for force for each distribution respectively. Neither is easily integrated with respect to both x (width of panel) and z (length of panel) directions, therefore both have been integrated with respect to z and then numerically integrated with respect to x using MATLAB's built in QUAD numerical integration function.

$$F_W = \frac{c(t)\pi\rho v_y{}^2}{2\tan\beta} 2\int_{x_c - r}^{x_c + r} \int_{z_c}^{z_c + \sqrt{r^2 - (x - x_c)^2}} \frac{1}{\sqrt{c(t)^2 - x^2}} dz dx \tag{6}$$

$$F_L = \frac{P_{\max}}{\frac{1}{\sqrt{1 - \frac{16(\tan\beta)^2}{\pi^2}}} - 1} 2\int_{x_c - r}^{x_c + r} \int_{Zc}^{Zc+} \sqrt{r^2 - (x - x_c)^2} \left(\frac{c(t)}{x} - 1\right) dz dx \tag{7}$$

The force can be converted back to a pressure by dividing by the sensing area of the pressure transducer. This area has been taken as the entire face of the pressure transducer which is circular with a radius of 2.81 mm, giving an area of 24.72 mm^2.

The theoretical predictions also need to be discretised at the same rate as the experimental data, 10 kHz or 20 kHz for these experiments depending on the impact velocity. The result of

this discretisation is a range of possible values, with upper and lower limits (Min Peak and Max Peak as indicated in Figure 7). The upper limit will is based on the possibility that the exact peak was captured as an experimental data point, while the lower limit is when the data point immediately before and after the peak pressure are of equal magnitude, creating the maximum variation between the corrected values and P_{max}. Figure 6 illustrates the possible variation in the peak based on the sampling rate. For comparisons with experimental data in this paper the maximum error theoretical prediction has been used. Similar consideration must be made for comparison of numerical results with either experimental data or theoretical predictions.

The error during the peak period of the impact is presented in Figure 8. The significant error at the start of the impact is due to the analytical prediction being zero, while the corrected solutions predict some pressure due to the average effects of the corrections undertaken. The maximum error is 50% which occurs close to the analytical peak. This error

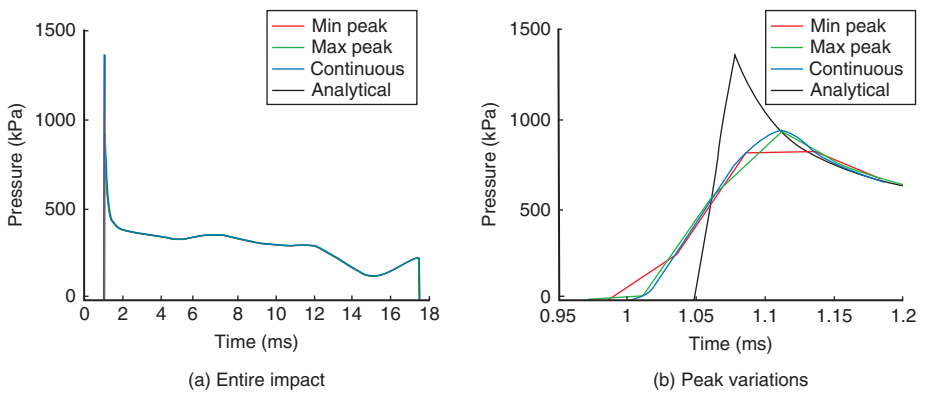

Figure 7 Theoretical predictions for pressure measured at x = 55 mm during a 6.0 m/s impact @ 10 deg with a 20 kHz sampling rate.

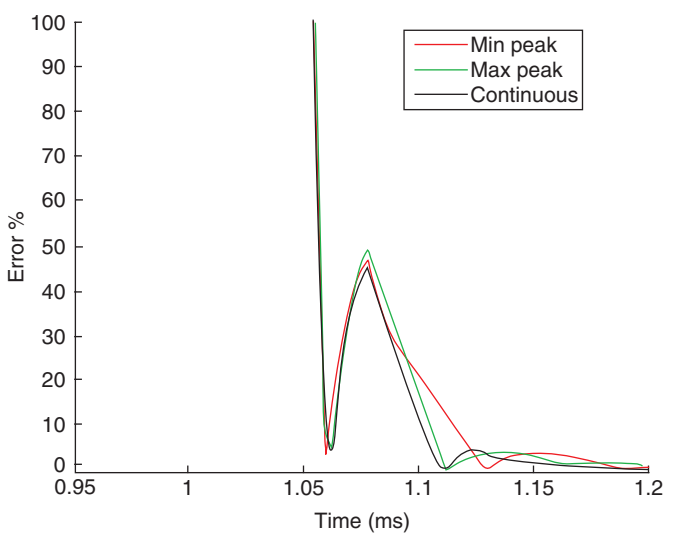

Figure 8 Errors for pressure measured at P1, x = 55 mm during a 6.0 m/s impact @ 10 deg with a 20 kHz sampling rate.

is not between the analytical and corrected peak values, which is closer to 30%. This difference arises from a phase shift in the pressure pulse between the analytical and corrected predictions. It should also be noted that after 1.1 ms there is less than 5% error, indicating the sensor size and sampling rate has little effect on the residual pressure measurement.

Figure 9 and Figure 10 show the significance of the transducer size on the pressure measurements during a 6 m/s impact at 10°. Figure 9 indicates that the ideal transducer size is as small as possible and that the error due to sensor size can increase rapidly with increasing sensing area. For instance an increase in transducer radius from 1.5 mm to 3 mm results in an 8.9 % increase in error at P1. The increase in area also has a greater effect at

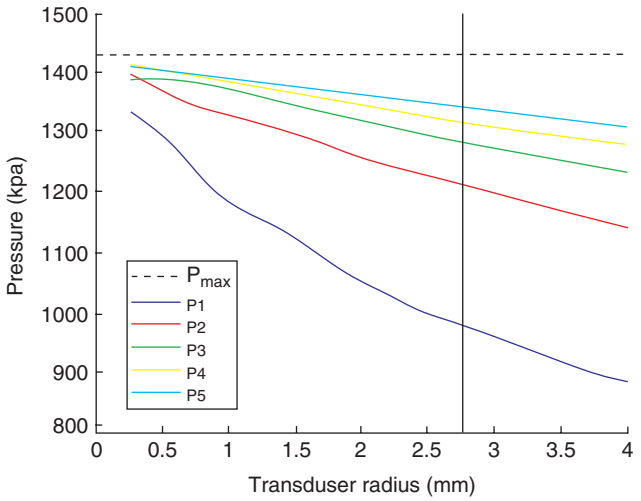

Figure 9 Theoretical pressures based on varying transducer radius, transducer radius used indicated (vertical black line).

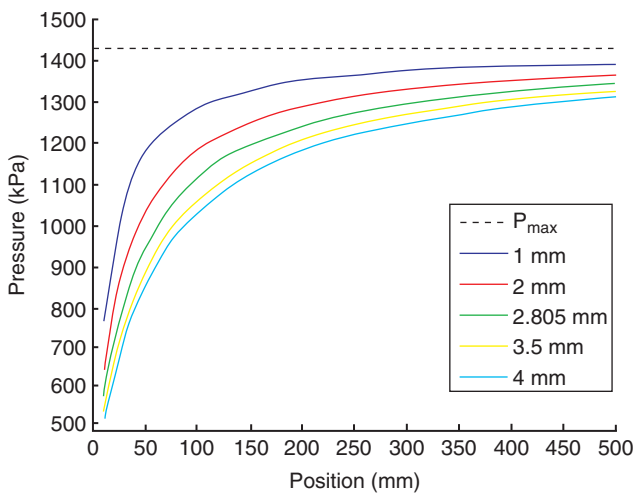

Figure 10 Theoretical pressures across the panel width for 5 different transducer sizes.

transducer locations closer to the keel (P1). For this series of tests the smallest transducer readily available was used to minimise these errors. The transducer radius of 2.805 mm is indicated on Figure 9 by the vertical black line. Figure 10 shows how the location of a pressure transducer on the panel affects the error in the measurement. For the measurements 100 mm from the edge of the panel the error is approximately 25% when using a transducer with a 2.805 mm radius. At 50mm the error increases to 38%. For measurements more than 250 mm from the keel of the panel there is much less error, dropping to 14%. This significant variation is important when comparing pressures taken at various locations across a panel's width, in order to ascertain if any variation is simply due to this measurement error or other phenomena.

3.3. COMPARISON OF EXPERRIMENT AND THEORY

Figure 11 to Figure 16 present the peak pressures from tests on three different panels at a range of impact velocties. This includes a nominally rigid panel, a carbon fibre/epoxy skin foam core sandwich panel with a flexural stiffness of 25,500 Nm and a glass fibre/epoxy skin foam core sandwich panel with a flexural stiffness of 6,740 Nm (C-C70.130 and G-C70.130 respectively in Table II). In Figure 11, Figure 13 and Figure 15 the experimental data is compared to Wagner's predicted peak pressures (equation 3) and the lower limit of the sensor area and sampling rate corrected prediction (as defined in Section 3.2). In Figure 12, Figure 14 and Figure 16 the same experimental data is normalised by the corrected peak pressure predictions. The results are presented for three pressure transducer positions, P1 (near to the keel edge of the panel), P3 (at the centre of the panel) and P5 (near to the chine edge of the panel), with exact positions defined in Figure 5.

For the case of transducer P1, Figure 11 shows that there is a significant difference between Wagner's analytical solution and the corrected predicted pressure magnitudes. This is due to the very narrow peak pressure pulse at this stage of the slamming event, which is particularly important for pressures measured close to the initial point of impact or for small panels. The experimental pressures from all three of the panels are similar to each other and demonstrate a similar trend as the Corrected predictions with pressure increases approximately proportional with velocity squared. There is however some variability in the

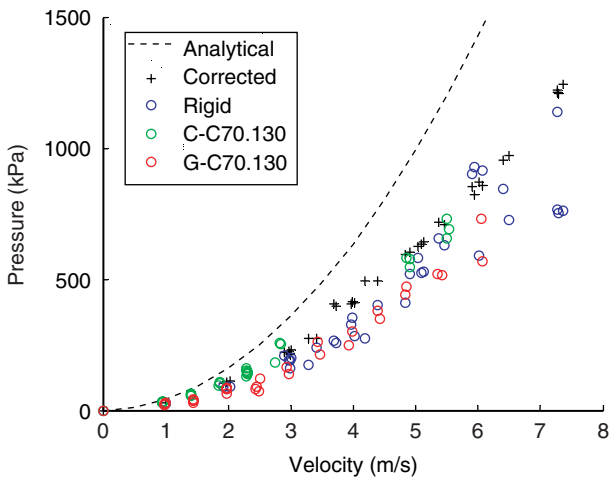

Figure 11 Peak pressure values for P1 (x = 55 mm).

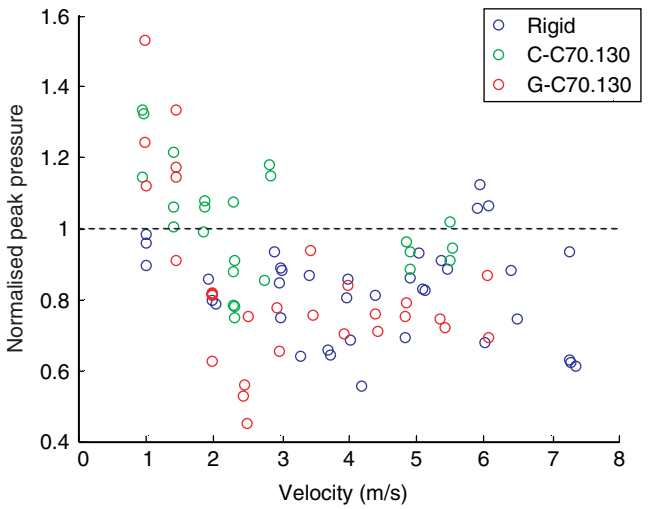

Figure 12 Normalised peak pressure values for P1 (x = 55 mm).

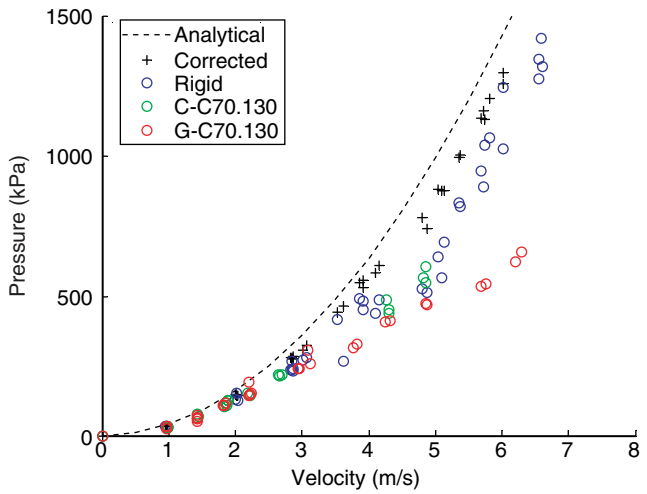

Figure 13 Peak pressure values for P3 (x = 270 mm).

results. Figure 2 presents the same experimental data for P1 normalised by the Corrected prediction. The significant scatter, and the fact that most of the results are lower than the Correct prediction demonstrates the difficulty in measuring pressures close to the point of initial impact due the narrower pressure peak. There does not appear to be any clear relationship between panel stiffness and pressure magnitude, presumably because the deflection is small close to the boundary of the panel at this early stage of the slamming event.

In the case of pressure transducer P3 (panel centre), Figure 13 shows that the differences between the Analytical and Corrected predictions are much smaller than for P1 due to the broader shape of the pressure peak. The pressures measured on the Rigid panel are slightly

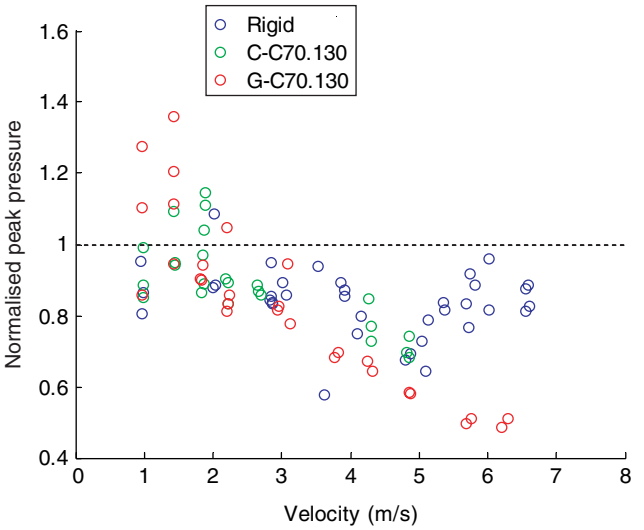

Figure 14 Normalised peak pressure values for P3 (x = 270 mm).

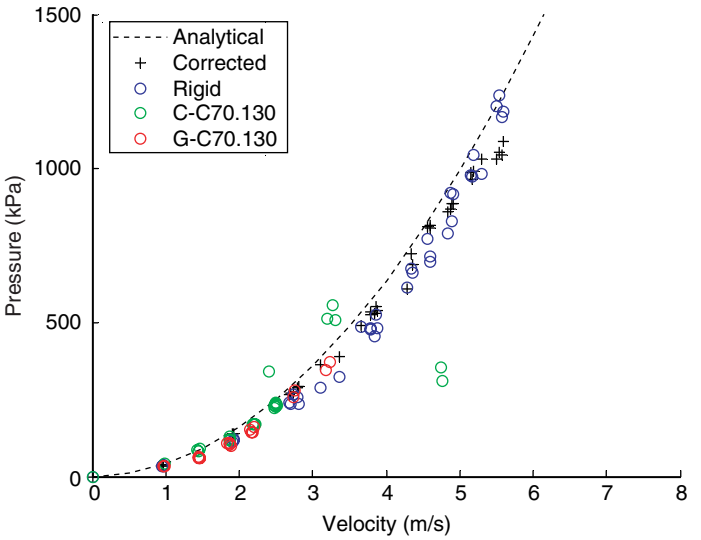

Figure 15 Peak pressure values for P5 (x = 485 mm).

lower (10 – 20 %), than the Corrected values. With the exception of a small group of tests around 4.5 m/s, the Rigid data follows the same trend as the Corrected values. The flexible panels, G-C70.130 and C-C70.130, both show a decreasing pressure relative to Corrected values which becomes more significant as the velocity increases. This is clearly shown in Figure 14 where the normalised peak pressure for both of the flexible panels decreases with increasing impact velocity. At low impact velocities the pressure measured on the most flexible panel (G-C70.130) is higher than the Corrected prediction by up to 40% while at higher velocities, above 5.5 m/s, the peak pressure decreases to 50% of the Corrected prediction. For the medium stiffness C-C70.130 panel, the pressures remain much closer to

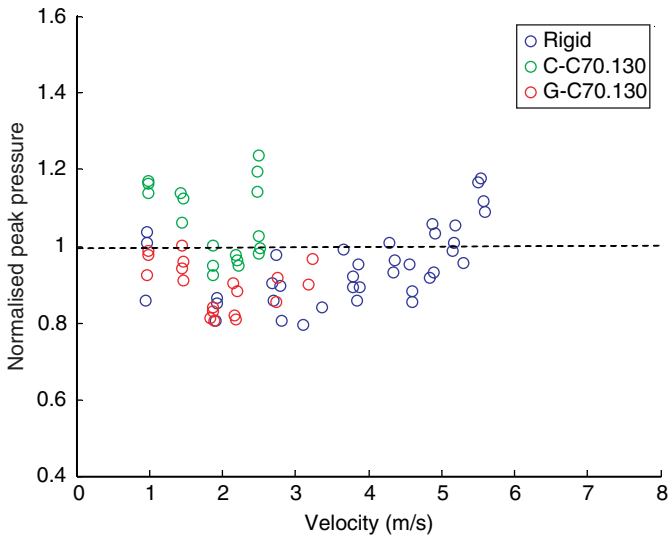

Figure 16 Normalised peak pressure values for P5 (x = 485 mm).

the Corrected values, however there is still a notable decrease in peak pressure to 70% of the predicted value at higher impact velocities. The lower flexural stiffness and therefore higher deflection of the G-C70.130 panel is the likely reason for the lower peak pressures.

Figure 15 shows that (with the exception of a few tests on the C-C70.130 panel), there is very little variation between the pressures measured at P5 for the three experimental panels and the pressures are similar to the predictions. The Analytical and Corrected predictions are only slightly different to each other because the pressure peak has become wider as the pulse moves across the panel to this sensor. The normalised results in Figure 16 show that there is up to approximately 20% variation in the experimental pressures compared to the Corrected theoretical prediction. There does not however appear to be any significant velocity related effect on the normalised peak pressures for any of the panels. This suggests that the flexibility of these panels do not influence the peak pressure at P5.

While the peak pressures are relatively easy to compare, they only act on each part of the panel for a small duration. The residual pressures act on the panel for much longer, and hence have a more significant effect on the panel responses. Because the residual pressure is not a discrete value it is necessary to define specific times to determine its magnitude. The approach taken here is to measure the residual pressure at the time at which the peak pressure reaches the subsequent pressure transducers. This means that the P1 residual pressure is determined when the peak pressure reaches P3 (17 ms in Figure 6), and the residual pressures at P1 and P3 are determined when the peak pressure occurs at P5 (26 ms in Figure 6).

Figure 17 shows the normalised residual pressure at P1 when the peak pressure reaches P3 for each of the panels. Figure 18 compares the normalised residual pressures at transducers P3 and P5 when the peak pressure has reached P5 for each of the panels. The pressures have been normalised against the theoretical residual pressures, as outlined in section 3.2.

Figure 17 shows that the residual pressures measured at P1 generally decrease with increasing velocity compared to the predicted pressures. The C-C70.130 panel appears to have a significant scatter in the data, which correlates with some oscillations observed in the

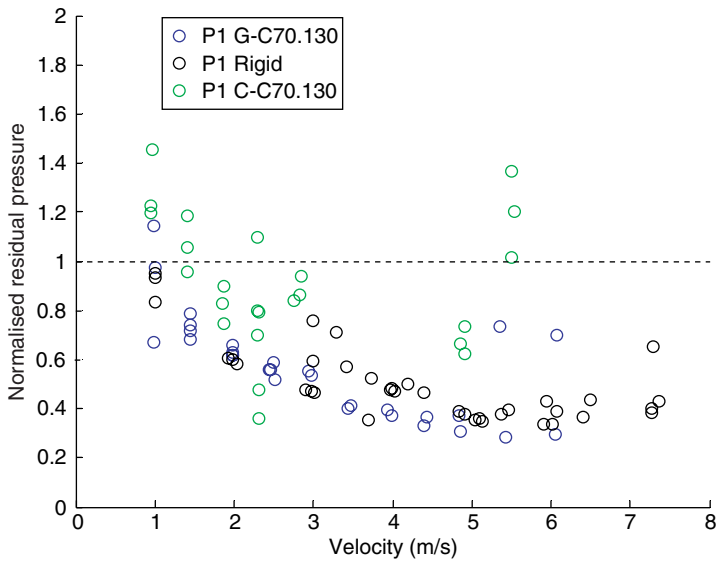

Figure 17 Normalised residual pressures when peak pressure is @ P3 (x = 270 mm).

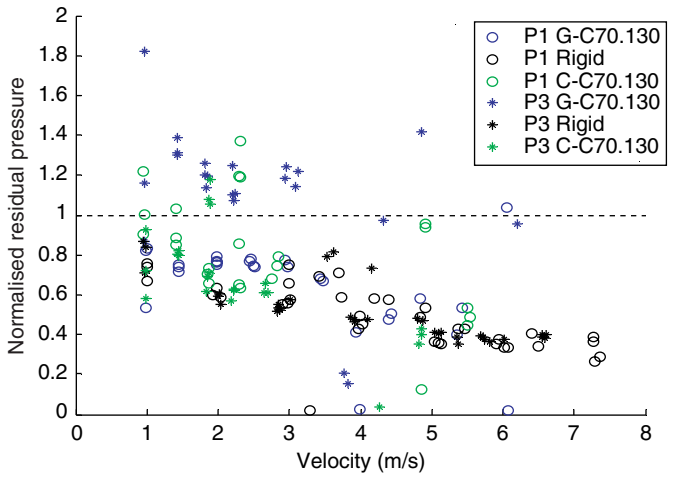

Figure 18 Normalised residual pressures when peak pressure is @ P5 (x = 485 mm).

residual pressures. The Rigid and G-C70.130 panels have a much clearer trend of decreasing normalised pressure with increasing impact velocity, with the measured pressure at velocities above 4 m/s being less than half the theoretical prediction. This indicates the theoretical residual pressure is over predicted at higher impact velocities. There appears to be no significant variation between the G-C70.130 and Rigid P1 residual pressures at this point, indicating there is little effect from the panels' flexibility.

Figure 18 shows the normalised residual pressures for P1 and P3 as measured when the peak pressure is at P5. The pressures measured from P1 on C-C70.130 panel show significant scatter similar to Figure 17, making interpretation difficult. The residual pressure measured

at P1 for the G-C70.130 and Rigid panels again shows a decreasing trend with increasing impact velocity. The flexible G-C70.130 panel does however consistently show slightly higher pressures at speeds between 1 and 3 m/s. The residual pressure measured at P3 varies for each of the panels. For the C-C70.130 panel there is significantly less scatter in the measured values. The Rigid and C-C70.130 pressures for P3 both have similar magnitudes to the P1 values measured from the rigid panel, with the exception of a few outliers. The G-C70.130 has substantially different residual pressure at P3 with all recorded pressures up to 3.5 m/s being above the predicted theoretical pressure. Considering the reasonable consistency of the measurements taken at both locations on the rigid panel and the pressures recorded at P1 on the G-C70.130, these increased residuals at P3 appear to indicate that the flexibility of the panel does influence the applied pressure at this position.

4. STRUCTURAL RESPONSES

4.1. TYPICAL STRUCTURAL REPONSES

The main slamming event takes place between water entry and full immersion, as shown in Figure 19 for slamming of the G-C70.130 panel at 3m/s and 10°. Pressures are measured at P1, P3 and P5, panel displacement at the centre of the panel (adjacent to P3), and strains measured on the inner panel skin at the centre (Strain 3, adjacent to P3) and near to the edge of the panel (Strain 5, adjacent to P5). The strain gauges are positioned 50 mm to the side of the pressure transducers.

The results show that the panel does not begin to deform until after the pressure pulse reaches P1 and that the maximum deformation of the panel occurs at a similar time as the pressure pulse reaches P5. This is expected, as at this stage the entire panel is being loaded, with most of the panel subjected to a distributed residual pressure, combined with the high pressure at the flow front near to the edge of the panel. The maximum strain at the centre of the panel (Strain 3) occurs slightly earlier than the maximum deflection, while there are only very small strains near to the edge of the panel (Strain 5) until quite late in the slamming event, but then this strain increases rapidly as the flow front nears the panel edge.

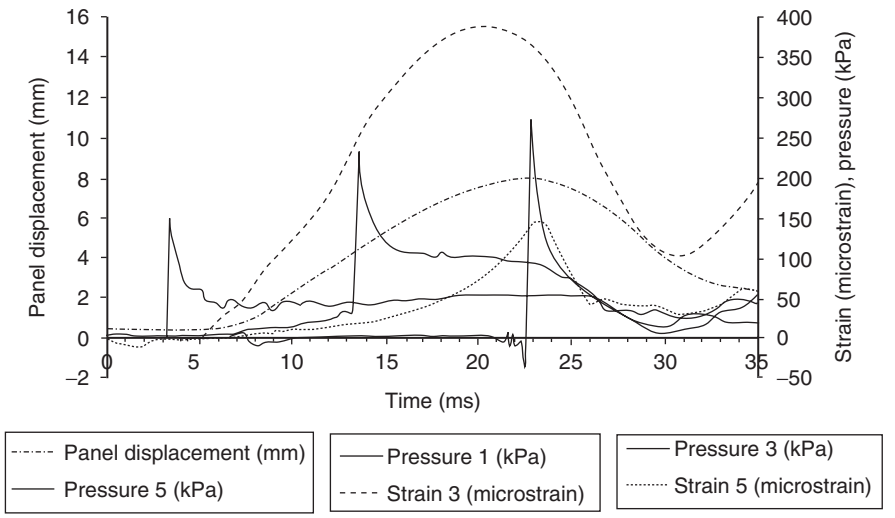

Figure 19 Pressures, strains and panel deformation time histories for slamming of the G-C70.130 panel at 3 m/s and 10°.

4.2. EFFECT OF PANEL COMPLIANCE ON ABSOLUTE RESPONSES

The structural response of the panel can be characterised through the strains measured on the inner skin of the panel. Strains at the panel centre are proportional to the applied moment at this position, and the strains near to the panel edge can also be used to estimate the resulting transverse shear force in this region [9].

Figure 20 and Figure 21 present the effect of impact velocity on strains at the centre and chine edge of the panels respectively. A second order trendline has been fitted to each of the sets of strain data. There is good correlation between the data and the trendlines, demonstrating that the strains are proportional to V^2 as expected since the pressure is proportional to velocity squared. The centre strains shown in Figure 20 follow the expected trend of increasing strain with reducing panel stiffness. The most flexible G-C70.130 panel has the highest strains, the thicker glass skin R63 core panels have lower strains, with the higher density cored R63.140 panel having slightly lower strains than the R63.80 panel. The carbon-fibre skinned C-C70.130 panel which has the highest flexural stiffness has the lowest strains.

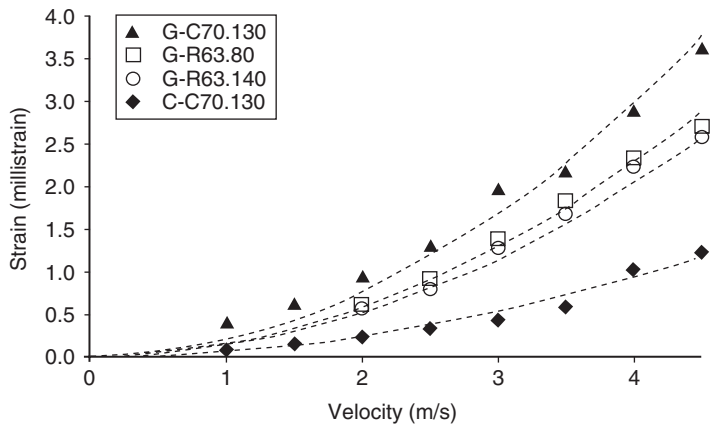

Figure 20 Strain at centre of panels (S3) relative to velocity.

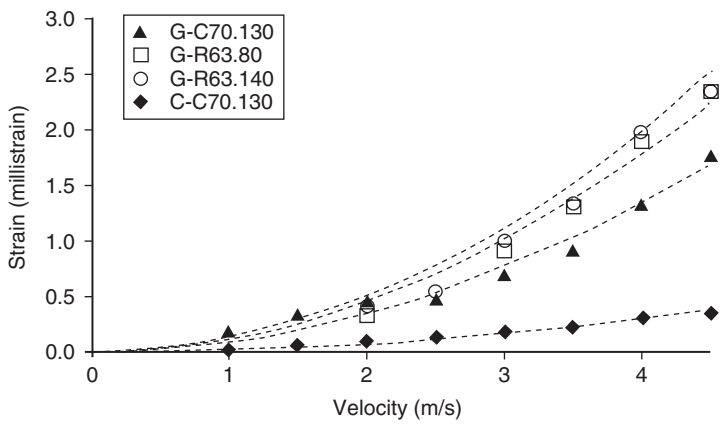

Figure 21 Strain at chine edge of panels (S5) at different velocity.

The relative strains at the chine (Figure 21) show a different trend, with the two R63 cored panels having the highest strains. The chine strains for both of the G-R63 panels are of similar magnitude to those at the centre, demonstrating the high local deformation in this region. The G-C70.130 panel has slightly lower strains than the other glass skinned panels. The carbon skinned C-C70.130 panel again has the lowest strains as expected.

Figure 22 presents the strains at the centre of the panel relative to the velocity squared, which is expected to be proportional to load. The experimental results correlate well with the first order trendlines confirming that the strains are proportional to the expected load. The same trend is evident for the strains at the chine edge, as shown in Figure 23.

4.3. COMPARISON TO ANALYTICAL PREDICTIONS

The measured strains can be compared to analytical predictions based on the expected mean pressure on the panel from Payne's formulation [4], combined with Kirchoff-Love plate theory series solution for simply supported panels from Zenkert [10]. Payne's formulation [4] is a calculation of the hydrodynamic force based on the conservation of momentum

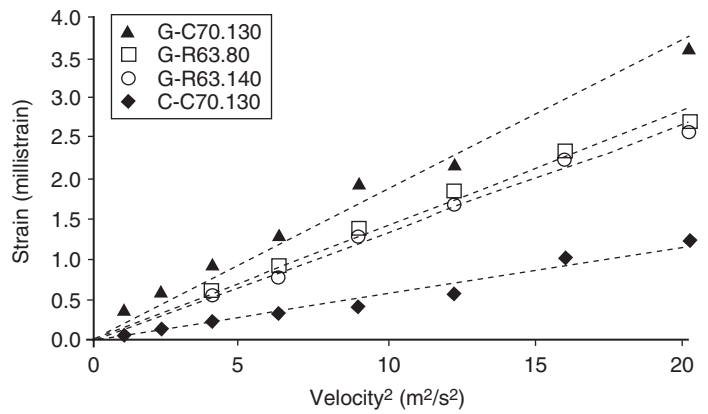

Figure 22 Strain at centre of panels (S3) relative to velocity squared.

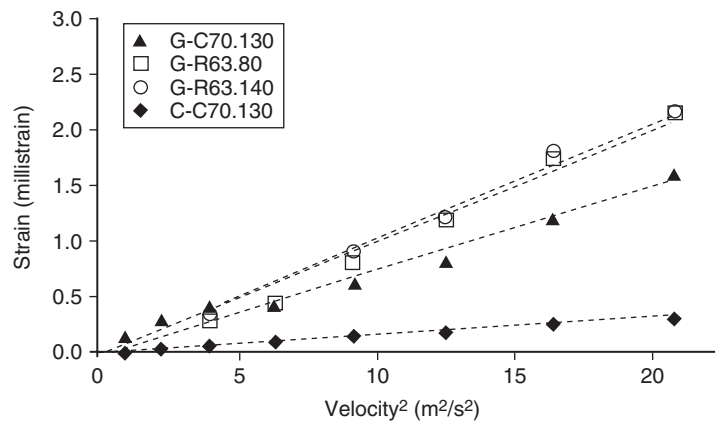

Figure 23 Strain at chine edge of panels (S5) relative to velocity squared.

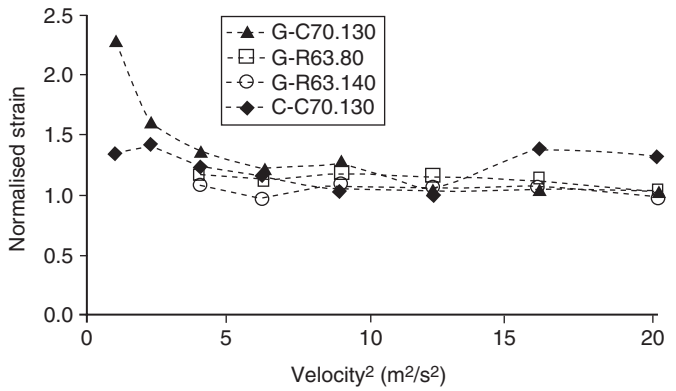

Figure 24 Normalised strain at centre of panels (S3) relative to velocity squared.

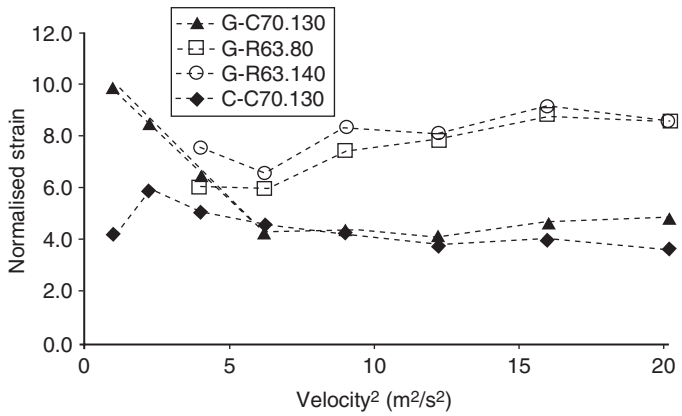

Figure 25 Normalised strain at chine edge of panels (S5) relative to velocity squared.

considering the mass of water displaced during the impact of a wedge into water. This force is then averaged across the panel to create an equivalent mean pressure.

Figure 24 and Figure 25 compare the resulting normalised strains at the centre and chine of the flexible panels to those expected on the basis of a uniform pressure load from Payne's solution. The results from the panels are normalised by dividing the experimental strains by the calculated strain based on a uniform equivalent pressure at each impact velocity. Hence a value of 1.0 would mean that the strain is the same as expected for the uniform pressure case and a value greater than 1.0 means that the experimental strain is higher than predicted.

Figure 24 shows that the strain at the centre of the panels is slightly higher than predicted for a uniform pressure case, particularly for smaller slamming impacts. The strain at the centre for the panels is between 1.0 and 1.5 times greater for all of the panels, apart from at very low impact velocities. There is little variation with respect to the impact velocity.

The moment at the chine of the panels (see Figure 25) is much higher than for the uniform case, with a maximum of approximately 10 times for the G-C70.130 panel at an impact velocity of 1 m/s. At high impact velocities the difference reduces, but is still 5 times that for the uniformly loaded case. Despite the large difference in flexural rigidity, the C-C70.130 panel has similar normalized strain values except for at low impact velocities. The G-R63.80

and G-R63.140 panels have similar normalized strains to each other, but much higher normalized strains than the C70 cored panels. The chine edge strain for the R63 cored panels is between 6 to 8 times the predicted value over the velocity range tested.

The high magnitude of the chine strains for all of these specimens is particularly important for sandwich panels because this is the position of maximum transverse shear force, and where core failure typically occurs.

5. CONCLUSIONS

While there has been significant development of numerical methods to simulate the fluid-structure interaction inherent in panel impact onto water there is only very limited experimental data available for validation of the simulation approaches. This study describes an experimental study of sandwich composite panels subjected to water slamming impacts to obtain results suitable for validation of multi-physics simulation methods. The work has two primary aims; to determine effects that the dimensions of pressure transducers and data acquisition sampling rates have on the measured pressures, and to characterise the effect that panel stiffness has on the pressures and responses for panel structures.

The results clearly demonstrate that the physical dimensions of pressure transducers and data acquisition sampling rates can have a significant effect on the measured pressures. For typical pressure transducers with a diameters of the order of a few mm the measured peak pressure can be more than 30% less than the theoretical maximum. The differences depend on the position of the transducer on the panel, with the errors being larger near to the keel edge of the panel where the pressure pulse initiates and reducing towards the chine edge of the panel as the pressure pulse becomes wider. The data acquisition sampling rate can also affect the maximum pressure measured, with rates of more than 20 kHz being required for the test conditions considered in this study. To compare experimental data to analytical or numerical prediction methods for validation it is essential to ensure that the results from each approach are compared for the equivalent transducer area and discretisation rates.

The magnitude of both peak and residual pressures are affected by the deformation of flexible panels, particularly at the centre of the panel. At this position the peak pressures are generally higher than analytical models and experimental data for rigid panels at low impact velocities, but reduce to be less than the rigid case at higher impact velocities as panel deformations increase. The peak pressure magnitudes do not appear to be significantly affected by the panel stiffness near to the keel and chine edges of the panel. The residual pressures at the panel centre increases for the more flexible panels, whereas it is generally lower than the analytical predictions near to the keel edge of the panel.

The non-uniform transient nature of the load and coupling between the deformation and the fluid loads results in the panels experiencing different strains than predicted for uniform pressure loads as typically used in design. Strains at the centre of the panels are proportional to the flexural stiffness of the specimens, however the strains at the edge of the panel do not show the same trend, and are affected by the core material type and panel thickness. The strain at the centre is relatively similar to that expected from classical uniform pressure based slamming analyses, but the strain close to the panel chine edge is much higher than predicted, in the cases tested up to 10 times the uniform pressure prediction. This results in higher than expected transverse shear forces, which can lead failure at the panel chine edge for sandwich structures.

ACKNOWLEDGEMENTS

This research has been financially supported by the USA Office of Naval Research (Grant N00014-08-1-0136) with Dr Y. Rajapakse as programme manager. The assistance of

Industrial Research Limited in providing access to the SSTS and SP-High Modulus (NZ) in providing technical guidance, materials supply and specimen manufacturing is also gratefully acknowledged.

REFERENCES

[1] Battley, M. and T. Allen (2011). "Servo-hydraulic System for Controlled Velocity Water Impact of Marine Sandwich Panels." *Experimental Mechanics*: pp1–12.

[2] Battley, M. and Stenius, I. 2003. "Dynamically Loaded Marine Composite Structures" presented at 14th International Conference on Composite Materials, San Diego, 14–18 July 2003.

[3] Stavovy, A.B. and S.-L. Chuang. 1976. "Analytical Determination of Slamming Pressures for High-Speed Vehicles in Waves," *Journal of Ship Research*, 20(4): 190–198.

[4] Payne, P.R. 1981. "The vertical impact of a wedge on a fluid," *Ocean Engineering*, 8(4): 421–436.

[5] Breder, J. 2005. "Experimental Testing of Slamming Pressure on a Rigid Marine Panel," Department of Aeronautical and Vehicle Engineering, Royal Institute of Technology, Stockholm.

[6] Downs-Honey, R., Edinger, S, and Battley, M. 2006. "Slam testing of Sandwich Panels", *SAMPE Journal*, 42(4).

[7] Battley, M. and Lake, S. 2006. "Designing Composite Structures for Slamming Loads", presented at the 2nd High Performance Yacht Design Conference, Auckland, February 14–16, 2006.

[8] Wagner, H., 1932 "Über Stoß- und Gleitvorgänge an der Oberfläche von Flüssigkeiten." *ZAMM - Zeitschrift für Angewandte Mathematik und Mechanik* 12(4): 193–215.

[9] Allen, T., and Battley, M. and Stenius, I. 2010. "Experimental Methods for Determining Shear Loads in Sandwich Structures Subjected to Slam Loading," presented at the *9th International Conference on Sandwich Structures*, Pasadena, June 14–16 2010.

[10] Zenkert, D. 1995. *An Introduction to Sandwich Construction*, EMAS Ltd, UK.